RESEARCH ARTICLE

Establishing a Spectral Optical CDMA System Involving the Use of Two Mutually Orthogonal States of Polarizations Using 1-D Two-Distinct Codes With Two-Code Keying

BIH-CHYUN YEH [ID]

Department of Electrical Engineering, College of Engineering, Chang Gung University, Taoyuan 33302, Taiwan
Department of Electrical and Computer Engineering, College of Engineering, Chang Gung University, Taoyuan 33302, Taiwan

e-mail: bih.chyun.yeh@gmail.com

ABSTRACT We propose 1-D Two-Distinct codes with two-code keying (TCK) using two mutually orthogonal states of polarization (SOP) in spectral components as a new code family for spectral amplitude coding (SAC) in optical code division multiple access (OCDMA) networks. Our proposed code structure operates the 1-D Two-Distinct codes with TCK using two mutually orthogonal SOP in spectral components to achieve a simple architecture. The modified cross-correlation within the 1-D Two-Distinct codes with TCK facilitates the transition from one code keying (OCK) to the generation of TCK. We design 1-D Two-Distinct codes with TCK to eliminate multiple user interference (MUI) caused by other simultaneous users through modified cross-correlation, thereby improving code operation. Although the recovered bits are affected by phase-induced intensity noise (PIIN), our proposed system can suppress PIIN. The numerical results show that our proposed system supports up to 45 simultaneous users and provides higher data transmission rates of 2.5 Gbps compared to other systems using 1-D SP codes with TCK, 1-D BIBD codes, and 1-D BDS codes with TCK.

INDEX TERMS Cross-correlation, multiuser interference, one code keying, optical code division multiple access, two code keying.

I. INTRODUCTION

Numerous researchers have investigated optical code-division multiple-access (OCDMA) systems because of their success in optical communications [1], [2], [3], [4], [5]. Spectral amplitude coding (SAC) schemes have provided a promising solution for applications affected by burst traffic environments in LANs. Recently, optical communications have been suggested for implementing SAC-optical code division multiple access (SAC-OCDMA) systems [6], [7], [8], [9], [10]. Central wavelengths were from address codes, which were generated from a broadband source using a

series of optical communications to produce spectral coding chips [11], [12], [13], [14], [15], [16]. However, OCDMA systems have long code lengths and the number of simultaneous users is limited by multiple-access interference (MUI). Among OCDMA systems, SAC systems have attracted particular attention because of their ability to eliminate MUI. Phase-induced intensity noise (PIIN) dominated the system performance owing to light waves at each photodiode [17], [18], [19], [20]. Each transmitter spread its code sequences to all receivers across the network.

Sahraouian et al. [21] established OCDMA as a significant technology in optical fiber communication, offering multiple attractive features through various encoding approaches. A new encoding technique utilizing multicore fibers was

---

The associate editor coordinating the review of this manuscript and approving it for publication was Daniel Augusto Ribeiro Chaves [ID].

proposed to generate code words while reducing the complexity of encoding and decoding methods. By sharing the signal power between cores, the nonlinearity effects were minimized, and the use of multicore fibers enhanced the system security. The solution using ZCC code produced an efficient null cross-correlation. Additionally, polarization with the solution affected the compounded bitrate and the number of simultaneous users. This allowed the sharing of the same code words by two users with different polarizations. This approach extended the capabilities of OCDMA to long-haul distances and high data rates beyond the access network.

Dam et al. [22] developed a novel encoding and decoding technique that took advantage of two orthogonal polarization states (vertical and horizontal) of optical code to increase the number of simultaneous users in FTTH networks. They applied SAC-OCDMA codes to both Optical Fiber Systems (OFS) and free-space optics (FSO). Multidimensional (MD) codes and cross-correlation values were utilized to test the effectiveness of incoherent SAC-OCDMA in FTTH networks. The simulation results revealed that the MD code outperformed the cross-correlation values in both OFS and FSO scenarios. Moreover, the MD codes performed better than the cross-correlation values at various distances in both OFS and FSO scenarios.

In this paper, a novel OCDMA approach is proposed that combines the two mutually orthogonal states of polarization (SOP) of the proposed Optical Line Terminal (OLT) to produce the proposed Optical Network Units (ONUs). The modified cross-correlation within the one-dimensional (1-D) Two-Distinct code with two-code keying (TCK) serves as a catalyst for transitioning from one-code keying (OCK) to the generation of TCK. The proposed system employs 1-D Two-Distinct codes with TCK using the modified cross-correlation to remove the MUI in a SAC-OCDMA system. A modified cross-correlation is used to overcome the MUI, which affects the performance of the OCDMA system. In addition, PIIN affects the system performance. The proposed 1-D Two-Distinct codes with TCK utilizes adjusted code sequences to evaluate and suppress PIIN. The numerical results of the proposed system using 1-D Two-Distinct codes with TCK are presented, including the number of simultaneous users, data transmission rate, and effective source power, which are 45, 2.5 Gbps, and −10 dBm, respectively. The proposed system using 1-D Two-Distinct codes with TCK has a higher number of simultaneous users, a higher data transmission rate, and a lower effective source power compared to the other systems using 1-D SP codes with TCK [23], 1-D BIBD codes [24], and 1-D BDS codes with TCK [25].

We recognize the non-existence of other systems using 1-D SP codes with TCK, 1-D BIBD codes, and 1-D BDS codes with TCK and introduce two mutually orthogonal SOP to improve the proposed system using 1-D Two-Distinct codes with TCK. This enhancement results in the adoption of TCK with two mutually orthogonal SOP in the proposed system. The methodology employed by the proposed system,

utilizing 1-D Two-Distinct codes with TCK, surpasses that of other systems utilizing 1-D SP codes with TCK, 1-D BIBD codes, and 1-D BDS codes with TCK. The proposed system generates 1-D Two-Distinct codes with OCK and transforms them into 1-D Two-Distinct codes with TCK. Consequently, the proposed system transitions from OCK to TCK by incorporating the use of two mutually orthogonal SOP. This approach differs from that of other systems using 1-D SP codes with TCK, 1-D BIBD codes, and 1-D BDS codes with TCK, which did not adopt the same method.

The remainder of this paper is structured as follows: In Section II, the design of the two mutually orthogonal SOP in the 1-D Two-Distinct codes with TCK is introduced. Section III presents the system architecture of the 1-D Two-Distinct codes with TCK. In Section IV, the equations and performance of the 1-D Two-Distinct codes with TCK in the OCDMA system are provided. Section V discusses the numerical results to increase the number of simultaneous users and data transmission rate and decrease the effective source power of 1-D Two-Distinct codes with TCK in the OCDMA system. Finally, in Section VI, the numerical results are discussed and presented for verification.

II. 1-D TWO-DISTINCT CODES WITH TCK

We utilize a matrix of 1-D codes through the introduction of 1-D Two-Distinct codes. The matrix of 1-D Two-Distinct codes is formed by taking the rows of the 1-D Two-Distinct codes with the code size and code length. The 1-D Two-Distinct codes exhibit a desirable property whereby any row of the matrix achieves an equal code weight, denoted by $\delta+1$, which is obtained from the code sequence. Constructing a matrix with 1-D Two-Distinct codes allows us to utilize the code size from each column. In particular, the code weight of the 1-D Two-Distinct codes is $\delta+1$ and the code length is $\delta^2 + \delta$, where the elements of the finite field GF(δ) over a prime δ are used to construct a sequence of integer numbers as follows:

$$p_{h,\delta} = \begin{cases} [(h + \kappa)(h + \mu) - \nu] \bmod \delta, & h = 0, 1, \ldots, \delta - 2, \\ [\kappa * \nu] \bmod \delta, & h = \delta - 1. \end{cases}$$

$$(1)$$

The sequence $p_{h,\delta}$ contains elements with parameters $h \in \{0, 1, 2, \ldots, \delta\text{-}1\}$, $\kappa \in \{0, 1, \ldots, \delta\text{-}1\}$, $\mu \in \{\delta\text{-}1, \delta\text{-}2, \ldots, 1, 0\}$, and $\nu \in \{\delta\text{-}1, \delta, \ldots, 0\}$. For each parameter pair (κ, μ, ν), the sequence $p_{h,\delta}$ is generated using the various parameters κ, μ, and ν. The code family can be determined based on the code weight $\delta+1$. By mapping the generated sequences $p_{h,\delta}$ to a binary number sequence (0, 1), the code sequence $q_{h,w}$ can be enhanced as follows:

$$q_{h,w} = \begin{cases} 1, & w = h\delta + p_{h,\delta}, \\ 0, & \text{otherwose.} \end{cases} \quad (2)$$

We propose incorporating 1-D Two-Distinct codes into the code sequence $q_{h,w}$ to achieve a code weight of $\delta+1$ and

TABLE 1. 1-D two-distinct codes with code weight $\delta = 3$.

Code Sequence											
0	1	0	0	0	1	0	0	1	0	1	0
0	0	1	1	0	0	1	0	0	0	1	0
1	0	0	0	1	0	0	1	0	0	1	0
0	0	1	0	0	1	0	1	0	0	0	1
1	0	0	1	0	0	0	0	1	0	0	1
0	1	0	0	1	0	1	0	0	0	0	1
0	0	1	0	1	0	0	0	1	1	0	0
1	0	0	0	0	1	1	0	0	1	0	0
0	1	0	1	0	0	0	1	0	1	0	0

TABLE 2. Cross-correlations of 1-D two-distinct codes.

Item	$c^{(0)}(h, g)$	$c^{(1)}(h, g)$
$h = 0 \cap g = 0$	$\delta + 1$	0
$h \neq 0 \cap g \neq 0$	1	δ

code length of $\delta^2 + \delta$. The value of h is an integer ranging from 0 to δ-1, and the sequence of a binary number (0, 1) is used to represent the code sequence $Q_h = \{q_{h,0}, q_{h,1}, \ldots, q_{h,\delta^2+\delta-1}\}$. Table 1 illustrates the code sequence of 1-D Two-Distinct codes for a code weight of 3.

The determination of the cross correlation is presented in Table 2. Cross-correlation $O_h^{(i)}$ is used for each user, and it exhibits a matrix that can be expressed as

$$C_{h,g}^{(0)} = Q_h^T * Q_g, \tag{3}$$

and

$$C_{h,g}^{(1)} = Q_h^T * \overline{Q_g}, \tag{4}$$

where the code sequence represented by Q_g and its complementary code sequence $\overline{Q_g}$ result in a cross-correlation $C_{h,g}^{(0)}$ and $C_{h,g}^{(1)}$. The cross-correlation $C_{h,g}^{(i)}$ can be written as

$$c^{(i)}(h, g) = \sum_{w=0}^{(\delta^2+\delta-1)} q_{h,w}^{(0)} q_{g,w}^{(i)}. \tag{5}$$

In this context, the component of the cross-correlation $C_{h,g}^{(0)}$ is from $c^{(0)}(h, g)$, whereas the component of the cross-correlation $C_{h,g}^{(1)}$ is from $c^{(1)}(h, g)$. By utilizing the definition of 1-D Two-Distinct codes, the code sequence $Q_g = \{q_{g,0}, q_{g,1}, \ldots, q_{g,\delta^2+\delta-1}\}$ and its complementary code sequence $\overline{Q_g} = \{\overline{q_{g,0}}, \overline{q_{g,1}}, \ldots, \overline{q_{g,\delta^2+\delta-1}}\}$ can be computed using the cross-correlation $C_{h,g}^{(0)}$ and $C_{h,g}^{(1)}$, as shown in (5).

Table 2 shows the cross-correlation, where $c^{(0)}(h, g)$ and $c^{(1)}(h, g)$ take on either nonzero or zero values. A nonzero value can be observed in $c^{(0)}(h, g)$ when $h = 0$ and $g = 0$. However, when $h \neq 0$ and $g \neq 0$, nonzero values are present in $c^{(0)}(h, g)$. Zero values can be detected in $c^{(1)}(h, g)$ when both h and g are equal to zero. However, nonzero values are also present in $c^{(1)}(h, g)$ when h is not set to 0 and g is not equal to 0. The values of $c^{(0)}(h, g)$ and $c^{(1)}(h, g)$ exhibit a fixed proportional relationship. Therefore, redundancy can be eliminated by using $c^{(0)}(h, g)$ and $c^{(1)}(h, g)$.

Cross-correlation interferences constitute MUI. Owing to the interference removed by $c^{(0)}(h, g)$ and $c^{(1)}(h, g)$, we proceed with the following steps to determine the desired property. To further reduce the interferences resulting from $c^{(0)}(h, g)$ and $c^{(1)}(h, g)$, we can express $c^{(0)}(h, g)$ and $c^{(1)}(h, g)$ in terms of

$$cc(h, g) = c^{(0)}(h, g) - c^{(1)}(h, g)/\delta. \tag{6}$$

As a result, when we obtain the cross-correlation $cc(h, g)$, $c^{(0)}(h, g)$ alleviates the interference caused by $c^{(1)}(h, g)$. Thus, $cc(h, g)$ is applicable when the values are nonzero or zero. By utilizing our formula, we can eliminate the interferences caused by $cc(h, g)$ by setting $h = 0$ and $g = 0$ or $h \neq 0$ and $g \neq 0$. From (7), we can suggest the following significant properties:

$$cc(h, g) = \begin{cases} (\delta + 1), & h = 0 \cap g = 0, \\ 0 & \text{otherwise.} \end{cases} \tag{7}$$

Equation (7) enables us to eliminate MUI and simultaneously mitigate PIIN.

We derived the adjusted cross-correlation $cc(h, g)$ when employing the first polarization in the polarizer. Next, we computed the cross-correlation $cc(h', g')$ using the second polarization in the polarizer as follows:

$$cc(h', g') = \begin{cases} (\delta + 1), & h' = 0 \cap g' = 0, \\ 0, & \text{otherwise.} \end{cases} \tag{8}$$

Therefore, we calculate the cross-correlation $cc(h, g)$ with the first polarization and cross-correlation $cc(h', g')$ with the second polarization, resulting in the TCK as follows:

$$cc(h, g) - cc(h', g')$$
$$= \begin{cases} (\delta + 1), & ib = 0 \cap h = 0 \cap g = 0, \\ -(\delta + 1), & ib = 1 \cap h' = 0 \cap g' = 0, \\ 0, & \text{otherwise,} \end{cases} \tag{9}$$

where ib is the information bit. $cc(h, g)$–$cc(h', g')$ represents a modified cross-correlation derived by deducting the

cross-correlation $cc(h, g)$ from the cross-correlation $cc(h', g')$. When the modified cross-correlation adheres to the constraints of $ib = 0$, $h = 0$, and $g = 0$, it yields a value of $(\delta + 1)$. Similarly, if the modified cross-correlation constraint is satisfied with $ib = 1$, $h' = 0$, and $g' = 0$, the outcome is $-(\delta + 1)$. In cases where there is no match, such as $ib = 0$, $h \neq 0$, and $g \neq 0$, or $ib = 1$, $h' \neq 0$, and $g' \neq 0$, the modified cross-correlation $cc(h, g)$–$cc(h', g')$ results in 0. Under the auto-modified cross-correlation constraint, when $ib = 0$, $h = 0$, and $g = 0$, the modified cross-correlation $cc(h, g)$–$cc(h', g')$ provides a value of $(\delta + 1)$. Conversely, for the other auto-modified cross-correlation constraint, where $ib = 1$, $h = h'$, and $g = g'$, $-(\delta + 1)$ is generated. However, interference from the MUI can disrupt communication with other users simultaneously. The modified cross-correlation takes advantage of its properties to eliminate this interference. The MUI elimination process involves the use of the MUI cancellation property of the modified cross-correlation $cc(h, g)$ - $cc(h', g')$ when employing 1-D Two-Distinct codes with TCK. In the context of the polarization SAC-OCDMA system, the proposed transmitters send information bits to the proposed receivers utilizing 1-D Two-Distinct codes with TCK. Upon receiving the code sequences associated with these 1-D Two-Distinct codes with TCK, the modified cross-correlation is employed to retrieve the recovered bits.

III. SYSTEM DESCRIPTION

The system diagram depicted in Fig. 1 comprises an OLT, $1 \times \delta^2$ polarization-maintaining splitter (PMS), and δ^2 ONUs. At the OLT, the data bits are modulated onto the optical signals, which are then transmitted to the $1 \times \delta^2$ PMS for distribution to δ^2 ONUs. The data bits correspond to the code sequences of 1-D Two-Distinct codes with TCK, and they are transmitted through the output of the OLT. The OLT provides two mutually orthogonal SOP that are combined with the spectral encoding of the 1-D Two-Distinct codes with TCK to form a single input to the $1 \times \delta^2$ PMS. The $1 \times \delta^2$ PMS also has two mutually orthogonal SOP with the spectral encoding of the 1-D Two-Distinct codes with TCK, and it has δ^2 connections to transmit the optical signals to the δ^2 ONUs. Consequently, the data bits, comprising two mutually orthogonal SOP with the spectral encoding of the 1-D Two-Distinct codes with TCK, are transmitted through the OLT, $1 \times \delta^2$ PMS, and δ^2 ONUs.

The diagram in Fig. 2 illustrates the construction of the proposed OLT. It consists of various components, including a broadband light source (BLS), polarizer, polarization controller, $1 \times \delta^2$ PMS with an equal power ratio, δ^2 sets of 1×2 polarization beam splitters (PBSs), $2\delta^2$ electro-optic modulators (EOMs), $2\delta^2$ optical circulators, $2\delta^2$ fiber Bragg gratings (FBGs), δ^2 sets of 2×1 polarization beam combiners (PBCs), and a $\delta^2 \times 1$ polarization-maintaining combiner (PMC) to encode the optical signal with the information bit. The BLS emits optical light, which is then polarized by the polarizer into two mutually orthogonal SOP, representing the vertical and horizontal orthogonal SOP. The polarization
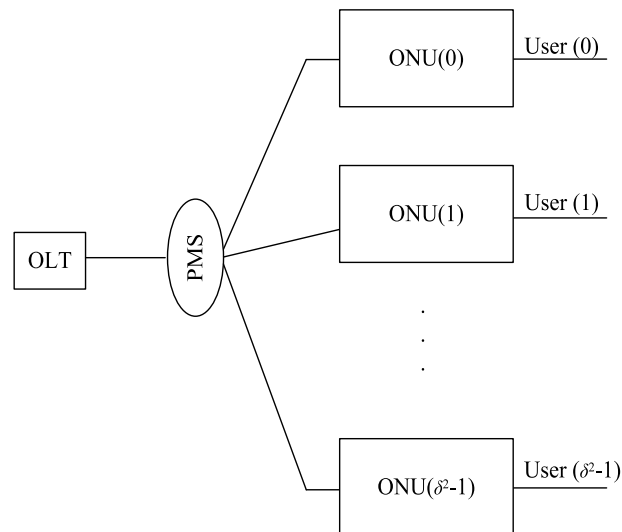

FIGURE 1. Schematic block diagram of 1-D Two-Distinct codes with TCK.

controller is used to produce an equal power ratio of two orthogonal SOP to correspond to two orthogonally polarized light beams specified as 1:1. The output of the polarization controller is then connected to the $1 \times \delta^2$ PMS, which splits the input into two mutually orthogonal SOP into δ^2 outputs in two mutually orthogonal SOP. This process is repeated for the $1 \times \delta^2$ PMS. The δ^2 outputs of the $1 \times \delta^2$ PMS are then linked to the δ^2 sets of the 1×2 PBSs. Each 1×2 PBS divides the vertical and horizontal orthogonal SOP into vertical orthogonal SOP of the up EOM and horizontal orthogonal SOP of the down EOM. Two connections between the two outputs of the 1×2 PBS and two inputs of the up and down EOM correspond to the vertical and horizontal orthogonal SOP. The two outputs of the 1×2 PBS are distributed to the two inputs of the up and down EOM, which are controlled by information bits. The two outputs of the up and down EOM are controlled by information bits to manipulate the two outputs of the up and down EOM.

The up EOM and down EOM are connected to two optical circulators and two FBGs. The reversing paths of the two optical circulators correspond to the complementary code sequences of the 1-D Two-Distinct codes with TCK, which reflect the spectral components based on the number of gratings in the two FBGs. Conversely, the passing paths of the two optical circulators align with the code sequences of the 1-D Two-Distinct codes with TCK, which pass through the spectral components based on the number of gratings in the two FBGs. The two FBGs are connected to two inputs of 2×1 PBCs, which polarize two mutually orthogonal SOP based on the passing paths of the two FBGs. Each 2×1 PBC polarizes two mutually orthogonal SOP with passing paths of two FBGs from two polarization states, that is, horizontal (0°) or vertical (90°) polarizations. The δ^2 outputs of the 2×1 PBCs are combined with the δ^2 inputs of $\delta^2 \times 1$ PMC. The output of $\delta^2 \times 1$ PMC is utilized as the output of the proposed OLT.
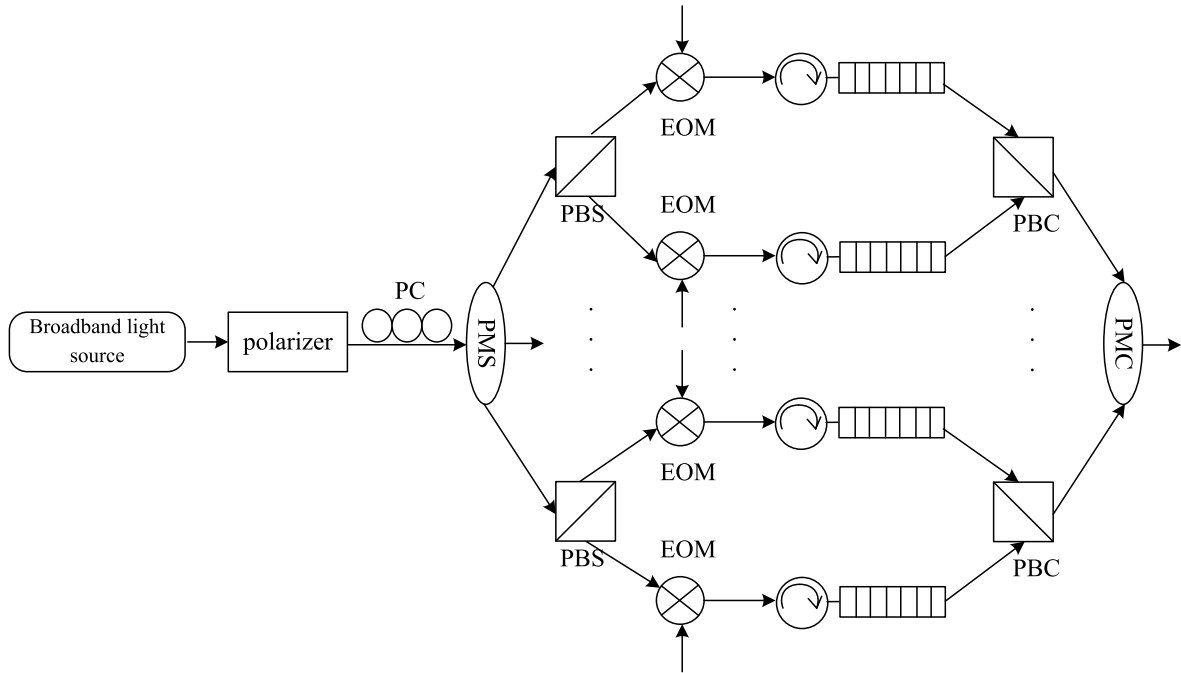
FIGURE 2. OLT structure of the proposed 1-D Two-Distinct codes with TCK OCDMA system.
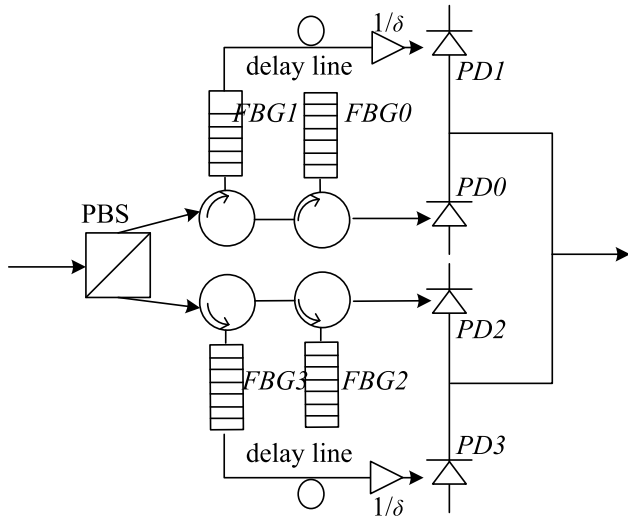

FIGURE 3. The ONU structure of the proposed 1-D Two-Distinct codes with TCK OCDMA system.

Figure 3 illustrates how the ONU is constructed, which includes a 1 × 2 PBS, four optical circulators, four sets of FBGs, two sets of delay lines, two sets of optical attenuators, and four photodiodes to recover the information bits of the optical signals. Initially, two polarizations with code sequences of the 1-D Two-Distinct codes with TCK are fed into the 1 × 2 PBS, which splits them into two sets of code sequences of the 1-D Two-Distinct codes with TCK. Two sets of code sequences of the 1-D Two-Distinct codes with TCK are then connected

to two outputs of the 1 × 2 PBS, which are further processed by two sets of up optical circulators, two sets of up FBGs, up delay line, up optical attenuator, two sets of up photodiodes, and two sets of down optical circulators, two sets of down FBGs, down delay line, down optical attenuator, and two sets of down photodiodes. Two sets of up optical circulators and down optical circulators are connected to two sets of up and down FBGs. The passing paths of the number of gratings in up FBG1 and down FBG3 are aligned with the complementary code sequences $\overline{Q_g^{(0)}}$ and complementary code sequence $\overline{Q_{g'}^{(0)}}$. Subsequently, the path proceeds to the up-delay line and down-delay line, eventually reaching the up-optical attenuator of $1/\delta$ and down optical attenuator of $1/\delta$, resulting in the generation of up photodiode PD1 and down photodiode PD3. Up FBG1 and down FBG3 are employed to selectively retrieve the reversing path of the number of gratings that correspond to '1s' in the spectral code sequence $Q_g^{(0)}$ and spectral code sequence $Q_{g'}^{(0)}$. Up FBG0 and down FBG2 are utilized to selectively capture the reversing path of the number of ratings corresponding to '1s' in the reversed spectral code sequences $Q_g^{(0)}$ and reversed spectral code sequence $Q_{g'}^{(0)}$, leading to the generation of the up photodiode PD0 and down photodiode PD2. However, their arrangements are entirely reversed to accommodate the round-trip delay compensation. Up FBG0 and up FBG1 are carefully designed to coincide with the reversed spectral code sequence $Q_g^{(0)}$, spectral code sequence $Q_g^{(0)}$, up delay line, and up optical attenuator of $1/\delta$, giving rise to photodiodes PD0 and PD1. In a meticulous design approach, down FBG2 and down FBG3 are precisely aligned with the reversed spectral

code sequence $Q_{g'}^{(0)}$, spectral code sequence $Q_{g'}^{(0)}$, down delay line, and down optical attenuator of $1/\delta$, resulting in down photodiodes PD2 and PD3.

As only the signal components that match the spectral code sequence of the proposed receiver can reach PD0, the output current of PD0 is directly proportional to $c^{(0)}(h, g)$. Similarly, the output currents of PDs 1–3 are proportional to $c^{(1)}(h, g)/\delta$, $c^{(0)}(h', g')$, and $c^{(1)}(h', g')/\delta$, respectively. Hence, the output currents of PD0, PD1, PD2, and PD3 are associated with $cc(h, g) = c^{(0)}(h, g) - c^{(1)}(h, g)/\delta$ and $cc(h', g') = [c^{(0)}(h', g') - c^{(1)}(h', g')/\delta]$, respectively. The overall output current of the receiver is determined as $cc(h, g)$–$cc(h', g')$. In summary, the output current of the receiver is proportional to $(\delta+1)$ for $ib = 0 \cap h = 0 \cap g = 0$, $-(\delta+1)$ for $ib = 1 \cap h' = 0 \cap g' = 0$, and otherwise as specified in (9). This arrangement allows the proposed receiver to successfully recover the desired data while effectively eliminating the MUI.

IV. PERFORMANCE ANALYSIS

Performance of the proposed system in calculating the bit error rate (BER) using Gaussian approximation. To determine the signal and noise, the signal-to-noise ratio (SNR) considers the signal power and noise power ratio, including the signal, thermal noise, shot noise, and PIIN in four photodiodes. The energy of the 1-D Two-Distinct codes with TCK is considered, which has cross-correlation to prevent overlapping spectra from different users. Several assumptions are made to simplify the calculation. First, the optical sources are assumed to have flat spectra across the bandwidth $[f_o - \Delta f/2, f_o + \Delta f/2]$, where f_o represents the central frequency and Δf represents the bandwidth of the source. Second, each power spectrum component has identical spectral widths. Third, each user has equal power at the proposed receiver. Finally, the bit streams generated by the distinct transmitters for each user reach the proposed receivers in synchronization.

All code sequences are included in the received optical signals to form the power spectral density (PSD), which can be expressed as:

$$\Theta(f) = \frac{P_{sr}}{\Delta f} \sum_{d=1}^{D} n(d) \sum_{w=0}^{\delta^2+\delta-1} (q_{h,w}^{(0)}) F(f, w). \quad (10)$$

Using this equation, we can obtain $\Theta(f)$, which depends on the effective power source P_{sr}, number of active users D, code length $\delta^2 + \delta$-1, and information bit ib (either '1' or '0') of the d-th user. The rect(i) function in (13) is defined as

$$F(f, w) = u\left[f - f_0 - \frac{\Delta f(-(\delta^2 + \delta) + 2w)}{2(\delta^2 + \delta)}\right]$$
$$- u\left[f - f_0 - \frac{\Delta f(-(\delta^2 + \delta) + 2w + 2)}{2(\delta^2 + \delta)}\right]. \quad (11)$$

The function $u(f)$ is the unit step function and is defined as:

$$u(f) = \begin{cases} 1, & f \geq 0, \\ 0, & f < 0. \end{cases} \quad (12)$$

The proposed system employs optical waves generated from the received optical signals using the PSD derived from the code sequences.

The proposed receivers utilize received optical signals to generate all code sequences. To compute the cross-correlation, the code sequence is multiplied by every code sequence, and the resulting products are summed together. Specifically, we calculate the cross-correlation between $c^{(0)}(h, g)$ and $c^{(1)}(h, g)$, as well as between $c^{(0)}(h', g')$ and $c^{(1)}(h', g')$ to obtain the results for the first, second, third, and fourth items, respectively. Cross-correlation is computed using the following equations over a one-bit period:

$$\Theta_{0,xbit}(f) = \frac{P_{sr}}{\Delta f} \sum_{d=1}^{D} n(d) \sum_{w=0}^{\delta^2+\delta-1} (q_{h,w,xbit}^{(0)}(d) q_{g,w,xbit}^{(0)}) F(f, w), \quad (13)$$

$$\Theta_{1,xbit}(f) = \frac{P_{sr}}{\delta \Delta f} \sum_{d=1}^{D} n(d) \sum_{w=0}^{\delta^2+\delta-1} (q_{h,w,xbit}^{(0)}(d) q_{g,w,xbit}^{(1)}) F(f, w), \quad (14)$$

$$\Theta_{2,xbit}(f) = \frac{P_{sr}}{\Delta f} \sum_{d=1}^{D} n(d) \sum_{w=0}^{\delta^2+\delta-1} (q_{h',w,,xbit}^{(0)}(d) q_{g',w,xbit}^{(0)}) F(f, w), \quad (15)$$

$$\Theta_{3,xbit}(f) = \frac{P_{sr}}{\delta \Delta f} \sum_{d=1}^{D} n(d) \sum_{w=0}^{\delta^2+\delta-1} (q_{h',w,xbit}^{(0)}(d) q_{g',w,xbit}^{(1)}) F(f, w), \quad (16)$$

where $c^{(0)}(h, g)$ represents the (h, g)th entry of the summation of cross-correlation $q_{h,w,xbit}^{(0)}(d) q_{g,w,xbit}^{(0)}$, $c^{(1)}(h, g)$ represents the (h, g)th entry of the summation of cross-correlation $q_{h,w,xbit}^{(0)}(d) q_{g,w,xbit}^{(1)}$, $c^{(0)}(h', g')$ represents the (h', g')-th entry of the summation of cross-correlation $q_{h',w,xbit}^{(0)}(d) q_{g',w,xbit}^{(0)}$, $c^{(1)}(h', g')$ represents the (h', g')-th entry of the summation of cross-correlation $q_{h',w,xbit}^{(0)}(d) q_{g',w,xbit}^{(1)}$, h ranges from 0 to δ^2-1, and g' ranges from 0 to δ^2-1. The value of $n(d)$, which is either zero or one, is determined by the information bit of the d-th user. If multiple users utilize the value $n(d) = 1$ to increase the information bits of the d-th user, it can lead to maximum interference, which results in MUI.

Assuming that the information bit ib is equal to zero and the use of photodiodes PD0, PD1, PD2, and PD3, the photocurrents $I_{PD0,xbit}$, $I_{PD1,xbit}$, $I_{PD2,xbit}$, and $I_{PD3,xbit}$ can be

described as follows:

$$I_{PD0,0bit} = R \int_0^\infty \Theta_{0,0bit}(f) df$$

$$= R \frac{P_{sr}}{\Delta f} \int_0^\infty \sum_{d=1}^D n(d) \sum_{w=0}^{\delta^2+\delta-1}$$

$$(q_{h,w,0bit}^{(0)}(d) q_{g,w,0bit}^{(0)}) F(f,w) df$$

$$= R \frac{P_{sr}}{\delta^2+\delta} \left[(\delta+1) + \frac{(\delta^2-1)(D-1)}{\delta^2-1} \right], \quad (17)$$

$$I_{PD1,0bit} = R \int_0^\infty \Theta_{1,0bit}(f) df$$

$$= R \frac{P_{sr}}{\delta \Delta f} \int_0^\infty \sum_{d=1}^D n(d) \sum_{w=0}^{\delta^2+\delta-1}$$

$$(q_{h,w,0bit}^{(0)}(d) q_{g,w,0bit}^{(1)}) F(f,w) df$$

$$= R \frac{P_{sr}}{\delta(\delta^2+\delta)} \left[\frac{\delta(\delta^2-1)(D-1)}{\delta^2-1} \right], \quad (18)$$

$$I_{PD0\_1,0bit} = R \int_0^\infty \left[\Theta_{0,0bit}(f) - \Theta_{1,0bit}(f) \right] df$$

$$= \left[I_{PD0,0bit} - I_{PD1,0bit} \right]$$

$$= R \frac{(\delta+1)P_{sr}}{\delta^2+\delta}, \quad (19)$$

$$I_{PD2,0it} = R \int_0^\infty \Theta_{2,0bit}(f) df$$

$$= R \frac{P_{sr}}{\delta^2+\delta} \left[\frac{(\delta^2-1)(D-1)}{\delta^2-1} \right], \quad (20)$$

$$I_{PD3,0bit} = R \int_0^\infty \Theta_{3,0bit}(f) df$$

$$= R \frac{P_{sr}}{\delta(\delta^2+\delta)} \left[\frac{\delta(\delta^2-1)(D-1)}{\delta^2-1} \right], \quad (21)$$

$$I_{PD2\_3,0bit} = R \int_0^\infty \left[\Theta_{2,0bit}(f) - \Theta_{3,0bit}(f) \right] df$$

$$= \left[I_{PD2,0bit} - I_{PD3,0bit} \right] = 0, \quad (22)$$

Or

In the case where the information bit *ib* is equal to 1, the following condition comes into effect:

$$I_{PD0,1bit} = R \int_0^\infty \Theta_{0,1bit}(f) df$$

$$= R \frac{P_{sr}}{(\delta^2+\delta)} \left[\frac{(\delta^2-1)(D-1)}{\delta^2-1} \right], \quad (23)$$

$$I_{PD1,1bit} = R \int_0^\infty \Theta_{1,1bit}(f) df$$

$$= R \frac{P_{sr}}{\delta(\delta^2+\delta)} \left[\frac{\delta(\delta^2-1)(D-1)}{\delta^2-1} \right], \quad (24)$$

$$I_{PD0\_1,1bit} = R \int_0^\infty \left[\Theta_{0,1bit}(f) - \Theta_{1,1bit}(f) \right] df$$

$$= \left[I_{PD0,1bit} - I_{PD1,1bit} \right] = 0, \quad (25)$$

$$I_{PD2,1bit} = R \int_0^\infty \Theta_{2,1bit}(f) df$$

$$= R \frac{P_{sr}}{\Delta f} \int_0^\infty \sum_{d=1}^D n(d) \sum_{w=0}^{\delta^2+\delta-1}$$

$$(q_{h',w,1bit}^{(0)}(d) q_{g',w,1bit}^{(0)}) F(f,w) df$$

$$= R \frac{P_{sr}}{\delta^2+\delta} \left[(\delta+1) + \frac{(\delta^2-1)(D-1)}{\delta^2-1} \right], \quad (26)$$

$$I_{PD3,1bit} = R \int_0^\infty \Theta_{3,1bit}(f) df$$

$$= R \frac{P_{sr}}{\delta \Delta f} \int_0^\infty \sum_{d=1}^D n(d) \sum_{w=0}^{\delta^2+\delta-1}$$

$$(q_{h',q,1bit}^{(0)}(d) q_{g'.w,1bit}^{(1)}) F(f,w) df$$

$$= R \frac{P_{sr}}{\delta(\delta^2+\delta)} \left[\frac{\delta(\delta^2-1)(D-1)}{\delta^2-1} \right], \quad (27)$$

$$I_{PD2\_3,1bit} = R \int_0^\infty \left[\Theta_{2,,1bit}(f) - \Theta_{3,1bit}(f) \right] df$$

$$= \left[I_{PD2,1bit} - I_{PD3,1bit} \right]$$

$$= R \frac{(\delta+1)P_{sr}}{\delta^2+\delta}. \quad (28)$$

The responsivity of the photodiode is given by $R = \eta e \lambda_o / hc$, where η is the quantum efficiency of the photodiode, e is the electron charge, λ_o is the wavelength at the center of the spectrum, h is Planck's constant, and c is the speed of light. The effective source power of each proposed receiver is denoted as P_{sr}. The photocurrents $I_{PD0,xbit}$, $I_{PD1,xbit}$, $I_{PD2,xbit}$, and $I_{PD3,xbit}$ are used to obtain the cross-correlations of $\Theta_{0,xbit}(f)$, $\Theta_{1,xbit}(f)$, $\Theta_{2,xbit}(f)$, $\Theta_{3,xbit}(f)$. The proposed receiver modifies the photocurrent, resulting in the following modified photocurrent:

Information bit $ib = 0$:

$$I_{PD,0bit} = I_{PD0\_1,0bit} - I_{PD2\_3,0bit} = R \frac{(\delta+1)P_{sr}}{\delta^2+\delta} - 0,$$

$$= R \frac{(\delta+1)P_{sr}}{\delta^2+\delta}, \quad (29)$$

Or

Information bit $ib = 1$:

$$I_{PD,1bit} = I_{PD0\_1,1bit} - I_{PD2\_3,1bit} = 0 - R \frac{(\delta+1)P_{sr}}{\delta^2+\delta},$$

$$= -R \frac{(\delta+1)P_{sr}}{\delta^2+\delta}. \quad (30)$$

The modified photocurrents correspond to the modified cross-correlations, which are subsequently used to recover the recovered bits.

To determine the photodiode noises, shot noise, PIIN, and thermal noise are considered. Because photocurrent noises have statistically independent characteristics, each noise source is considered independently. The photocurrent noise variances, including the shot noise variance,

PIIN variance, and thermal noise variance, are calculated. By detecting the variance of these noise sources, the photodiode noise can be expressed as photocurrent noise variances [14].

$$
\left\langle i^2_{noise,xbit} \right\rangle = \left\langle i^2_{PIIN,xbit} \right\rangle + \left\langle i^2_{shot,xbit} \right\rangle + \left\langle i^2_{thermal,xbit} \right\rangle
$$
$$
= B_r I^2_{PD}\tau_a + 2eI_t B_r + 4K_a T_n B_r/RL. \quad (31)
$$

The parameters used in Eq.(31) are incorporated into the above equation. The photocurrent analysis considers the variance powers of PIIN, shot noise, and thermal noise, which include the average photocurrent I_{PD} (A), total photocurrent I_{total} (A), electrical bandwidth B_r (Hz), coherence time of the light incident on the photodiode τ_a (s), electron charge e (C), Boltzmann's constant K_a, absolute noise temperature T_n (K), and load resistance R_L (Ω). Therefore, τ_a can be expressed as follows [17]:

$$
\tau_a = \left(\int_0^\infty \Theta^2(f)df \right) \Big/ \left(\int_0^\infty \Theta(f)df \right)^2. \quad (32)
$$

$\Theta(f)$ is the light that reaches the photodiode using the PSD of single-sideband light. The photocurrent noise variances are calculated based on the statistically independent noise characteristics of shot noise, PIIN, and thermal noise.

The expression for the PIIN variance is presented below:

$$
\left\langle i^2_{PIIN,xbit} \right\rangle = B_r I^2_{PD}\tau_a. \quad (33)
$$

The electrical bandwidth is denoted by B_r, whereas the coherence time of the light incident on the photodiode is represented by τ_a. PIIN variance can be expressed as (34) and (35), shown at the bottom of the page. where $\Theta_{0,0bit}(f)$ denotes the cross-correlation and $\Theta_{1,0bit}(f)$ denotes its complementary cross-correlation. Additionally, $\Theta_{2,0bit}(f)$ represents the cross-correlation and $\Theta_{3,0bit}(f)$ represents its complementary cross-correlation. Subsequently, we obtain the following:

Information bit $ib = 0$ bit:

$$
\left\langle i^2_{PIIN,0bit} \right\rangle
$$
$$
= R^2 B_r \int_0^\infty \Big[\Theta^2_{0,0bit}(f) + \Theta^2_{1,0bit}(f) + \Theta^2_{0,0bit}(f) + \Theta^2_{1,0bit}(f)
$$
$$
- 2\Theta_{0,0bit}(f)\Theta_{2,0bit}(f) - 2\Theta_{1,0bit}(f)\Theta_{3,0bit}(f) \Big] df, \quad (36)
$$

or Information bit $ib = 1$ bit:

$$
\left\langle i^2_{PIIN,1bit} \right\rangle
$$
$$
= R^2 B_r \int_0^\infty \Big[\Theta^2_{0,1bit}(f) + \Theta^2_{1,1bit}(f) + \Theta^2_{2,1bit}(f) + \Theta^2_{3,1bit}(f)
$$
$$
- 2\Theta_{0,1bit}(f)\Theta_{2,1bit}(f) - 2\Theta_{1,1bit}(f)\Theta_{3,1bit}(f) \Big] df, \quad (37)
$$

where $\Theta_{0,1bit}(f)$ denotes the cross-correlation and $\Theta_{1,1bit}(f)$ denotes its complementary cross-correlation. Additionally, $\Theta_{2,1bit}(f)$ represents the cross-correlation and $\Theta_{3,1bit}(f)$ represents its complementary cross-correlation. The square of the spectrum with $\Theta_{0,xbit}(f)$, $\Theta_{1,xbit}(f)$, $\Theta_{2,xbit}(f)$, $\Theta_{3,xbit}(f)$, and the spectrum with $2\Theta_{0,xbit}(f)\Theta_{0,xbit}(f)$, and $2\Theta_{0,xbit}(f)\Theta_{0,xbit}(f)$, based on the PIIN variance, involves integral calculus with frequency. Equations (38)–(43) provide the integrals as the information bit $ib = 0$ bit.

$$
\int_0^\infty \Theta^2_{0,0bit}(f)df
$$
$$
= \frac{P^2_{sr}}{\Delta f^2} \int_0^\infty \left[\sum_{d=1}^{D} n(d) \sum_{w=0}^{\delta^2+\delta-1} (q^{(0)}_{h,w,0bit} q^{(0)}_{g,w,0bit})F(f,w) \right]^2 df
$$
$$
= \frac{P^2_{sr}}{\Delta f(\delta^2+\delta)(\delta+1)} \left[(\delta+1) + \frac{(\delta+1)(\delta-1)(D-1)}{\delta^2-1} \right]^2 \quad (38)
$$

$$
\int_0^\infty \Theta^2_{1,0bit}(f)df
$$
$$
= \frac{P^2_{sr}}{\delta^2 \Delta f^2} \int_0^\infty \left[\sum_{d=1}^{D} n(d) \sum_{w=0}^{\delta^2+\delta-1} (q^{(0)}_{h,w,0bit} q^{(1)}_{g,w,0bit})F(f,w) \right]^2 df
$$
$$
= \frac{P^2_{sr}}{\Delta f(\delta^2+\delta)\delta^2(\delta^2-1)} \left[\frac{(\delta^2-1)\delta(D-1)}{\delta^2-1} \right]^2, \quad (39)
$$

$$
\int_0^\infty \Theta^2_{2,0bit}(f)df
$$
$$
= \frac{P^2_{sr}}{\Delta f^2} \int_0^\infty \left[\sum_{d=1}^{D} n(d) \sum_{w=0}^{\delta^2+\delta-1} (q^{(0)}_{h',w,0bit} q^{(0)}_{g',w,0bit})F(f,w) \right]^2 df
$$
$$
= \frac{P^2_{sr}}{\Delta f(\delta^2+\delta)(\delta+1)} \left[\frac{(\delta+1)(\delta-1)(D-1)}{\delta^2-1} \right]^2, \quad (40)
$$

$$
\left\langle i^2_{PIIN,0bit} \right\rangle = B_r I^2_{PD} \frac{\int_0^\infty \left[\Theta_{0,0bit}(f) - \Theta_{1,0bit}(f) - \Theta_{2,0bit}(f) + \Theta_{3,0bit}(f) \right]^2 df}{\left(\int_0^\infty \left[\Theta_{0,0bit}(f) - \Theta_{1,0bit}(f) - \Theta_{2,0bit}(f) + \Theta_{3,0bit}(f) \right] df \right)^2}, \quad (34)
$$
$$
= R^2 B_r \int_0^\infty \Big[\Theta^2_{0,0bit}(f) + \Theta^2_{1,0bit}(f) + \Theta^2_{2,0bit}(f) + \Theta^2_{3,0bit}(f)
$$
$$
- 2\Theta_{0,0bit}(f)\Theta_{1,0bit}(f) - 2\Theta_{0,0bit}(f)\Theta_{2,0bit}(f) + 2\Theta_{0,0bit}(f)\Theta_{3,0bit}(f)
$$
$$
+ 2\Theta_{1,0bit}(f)\Theta_{2,0bit}(f) - 2\Theta_{1,0bit}(f)\Theta_{3,0bit}(f) - 2\Theta_{2,0bit}(f)\Theta_{3,0bit}(f) \Big] df, \quad (35)
$$

$$\int_0^\infty \Theta_{3,0bit}^2(f)df$$

$$= \frac{P_{sr}^2}{\delta^2 \Delta f^2} \int_0^\infty \left[\sum_{d=1}^D n(d) \sum_{w=0}^{\delta^2+\delta-1} (q_{h',w,0bit}^{(0)} q_{g',w,0bit}^{(1)}) F(f,w) \right]^2 df$$

$$= \frac{P_{sr}^2}{\Delta f(\delta^2+\delta)\delta^2(\delta^2-1)} \left[\frac{(\delta^2-1)\delta(D-1)}{\delta^2-1} \right]^2, \qquad (41)$$

$$\int_0^\infty 2\Theta_{0,0bit}(f)\Theta_{2,0bit}(f)df$$

$$= \frac{2P_{sr}^2}{\Delta f^2} \int_0^\infty \left[\sum_{d=1}^D n(d) \sum_{w=0}^{\delta^2+\delta-1} (q_{h,w,0bit}^{(0)} q_{g,w,0bit}^{(0)}) F(f,w) \right]$$

$$* \left[\sum_{d=1}^D n(d) \sum_{w=0}^{\delta^2+\delta-1} (q_{h',w,0bit}^{(0)} q_{g',w,0bit}^{(0)}) F(f,w) \right] df$$

$$= \frac{2P_{sr}^2}{\Delta f(\delta^2+\delta)(\delta+1)} \left[(\delta+1) + \frac{(\delta+1)(\delta-1)(D-1)}{\delta^2-1} \right]$$

$$* \left[\frac{(\delta+1)(\delta-1)(D-1)}{\delta^2-1} \right], \qquad (42)$$

$$\int_0^\infty 2\Theta_{1,0bit}(f)\Theta_{3,0bit}(f)df$$

$$= \frac{2P_{sr}^2}{\delta \Delta f^2} \int_0^\infty \left[\sum_{d=1}^D n(d) \sum_{w=0}^{\delta^2+\delta-1} (q_{h,w,0bit}^{(0)} q_{g,w,0bit}^{(1)}) F(f,w) \right]$$

$$* \left[\sum_{d=1}^D n(d) \sum_{w=0}^{\delta^2+\delta-1} (q_{h',w,,0bit}^{(0)} q_{g',w,0bit}^{(1)}) F(f,w) \right] df$$

$$= \frac{2P_{sr}^2}{\Delta f(\delta^2+\delta)\delta(\delta^2-1)} \left[\frac{(\delta^2-1)\delta(D-1)}{\delta^2-1} \right]$$

$$* \left[\frac{(\delta^2-1)\delta(D-1)}{\delta^2-1} \right], \qquad (43)$$

or Information bit $ib = 1$ bit:

$$\int_0^\infty \Theta_{0,1bit}^2(f)df$$

$$= \frac{P_{sr}^2}{\Delta f^2} \int_0^\infty \left[\sum_{d=1}^D n(d) \sum_{w=0}^{\delta^2+\delta} (q_{h,w,1bit}^{(0)} q_{g,w,1bit}^{(0)}) F(f,w) \right]^2 df$$

$$= \frac{P_{sr}^2}{\Delta f(\delta^2+\delta)(\delta+1)} \left[\frac{(\delta+1)(\delta-1)(D-1)}{\delta^2-1} \right]^2, \qquad (44)$$

$$\int_0^\infty \Theta_{1,1bit}^2(f)df$$

$$= \frac{P_{sr}^2}{\delta^2 \Delta f^2} \int_0^\infty \left[\sum_{d=1}^D n(d) \sum_{w=0}^{\delta^2+\delta-1} (q_{h,w,1bit}^{(0)} q_{g,w,1bit}^{(1)}) F(f,w) \right]^2 df$$

$$= \frac{P_{sr}^2}{\Delta f(\delta^2+\delta)\delta^2(\delta^2-1)} \left[\frac{(\delta^2-1)\delta(D-1)}{\delta^2-1} \right]^2, \qquad (45)$$

$$\int_0^\infty \Theta_{2,1bit}^2(f)df$$

$$= \frac{P_{sr}^2}{\Delta f^2} \int_0^\infty \left[\sum_{d=1}^D n(d) \sum_{w=0}^{\delta^2+\delta-1} (q_{h',w,1bit}^{(0)} q_{g',w,1bit}^{(0)}) F(f,w) \right]^2 df$$

$$= \frac{P_{sr}^2}{\Delta f(\delta^2+\delta)(\delta+1)} \left[(\delta+1) + \frac{(\delta+1)(\delta-1)(D-1)}{\delta^2-1} \right]^2, \qquad (46)$$

$$\int_0^\infty \Theta_{3,1bit}^2(f)df$$

$$= \frac{P_{sr}^2}{\delta^2 \Delta f^2} \int_0^\infty \left[\sum_{d=1}^D n(d) \sum_{w=0}^{\delta^2+\delta-1} (q_{h',w,1bit}^{(0)} q_{g',w,1bit}^{(1)}) F(f,w) \right]^2 df$$

$$= \frac{P_{sr}^2}{\Delta f(\delta^2+\delta)\delta^2(\delta^2-1)} \left[\frac{(\delta^2-1)\delta(D-1)}{\delta^2-1} \right]^2, \qquad (47)$$

$$\int_0^\infty 2\Theta_{0,1bit}(f)\Theta_{2,1bit}(f)df$$

$$= \frac{2P_{sr}^2}{\Delta f^2} \int_0^\infty \left[\sum_{d=1}^D n(d) \sum_{w=0}^{\delta^2+\delta-1} (q_{h,w,1bit}^{(0)} q_{g,w,1bit}^{(0)}) F(f,w) \right]$$

$$* \left[\sum_{d=1}^D n(d) \sum_{w=0}^{\delta^2+\delta-1} (q_{h',w,1bit}^{(0)} q_{g',w,1bit}^{(0)}) F(f,w) \right] df$$

$$= \frac{2P_{sr}^2}{\Delta f(\delta^2+\delta)(\delta+1)} \left[\frac{(\delta+1)(\delta-1)(D-1)}{\delta^2-1} \right]$$

$$* \left[(\delta+1) + \frac{(\delta+1)(\delta-1)(D-1)}{\delta^2-1} \right], \qquad (48)$$

$$\int_0^\infty 2\Theta_{1,1bit}(f)\Theta_{3,1bit}(f)df$$

$$= \frac{2P_{sr}^2}{\delta \Delta f^2} \int_0^\infty \left[\sum_{d=1}^D n(d) \sum_{w=0}^{\delta^2+\delta-1} (q_{h,w,1bit}^{(0)} q_{g,w,1bit}^{(1)}) F(f,w) \right]$$

$$* \left[\sum_{d=1}^D n(d) \sum_{w=0}^{\delta^2+\delta-1} (q_{h',w,1bit}^{(0)} q_{g',w,1bit}^{(1)}) F(f,w) \right] df$$

$$= \frac{2P_{sr}^2}{\Delta f(\delta^2+\delta)\delta(\delta^2-1)} \left[\frac{(\delta^3-1)\delta(D-1)}{\delta^2-1} \right]$$

$$* \left[\frac{(\delta^2-1)\delta(D-1)}{\delta^2-1} \right]. \qquad (49)$$

We integrate (38)–(49) with frequency. Considering that all users send a recovered bit of "0," the PIIN variance is obtained. Hence, the value of $\langle i_{PIID,0bit}^2 \rangle$ corresponds to a recovered bit of "0." The $\langle i_{PIID,1bit}^2 \rangle$ transmits a recovered bit "1" to generate the PIIN variance. The (38) and (49) are obtained by utilizing the PIIN variances for $\langle i_{PIID,0bit}^2 \rangle$ and $\langle i_{PIID,1bit}^2 \rangle$. As a result, the proposed system is capable of recovering the recovered bits "0" or "1" with equal probability using the PIIN variance.

The shot noise is caused by the random fluctuation of electron charges. This affects the random fluctuation energy and results in shot noise variance that possesses statistically independent noise characteristics. Considering the influence of the electron charge on the shot noise, the equation for shot noise variance is derived as follows:

$$\left\langle i^2_{shot,0bit} \right\rangle = 2eB_r I_{t,0bit}, \tag{50}$$

or

$$\left\langle i^2_{shot,1bit} \right\rangle = 2eB_r I_{t,1bit}. \tag{51}$$

The total photocurrents $I_{t,0bit}$ and $I_{t,1bit}$ are obtained by adding $I_{PD0,0bit}$, $I_{PD1,0bit}$, $I_{PD2,0bit}$, $I_{PD3,0bit}$, and $I_{PD0,1bit}$, $I_{PD1,1bit}$, $I_{PD2,1bit}$, $I_{PD3,1bit}$, respectively. The recovered bits "0" and "1" are equally likely for each user, and we use them to calculate the shot noise variance, leading to the derivation of (50) and (51). This ensures that the recovered bits "0" and "1" have equal probability for every user.

Thermal noise is determined by the electrical bandwidth B_r, which converts into thermal noise energy and is known as the thermal noise variance. The thermal noise variance is computed using Boltzmann's constant K_a, absolute noise temperature T_n in degrees Kelvin (K), electrical bandwidth B_r, and load resistance R_L (Ohm). The expression for the thermal noise variance is given by

$$\left\langle i^2_{thermal,0bit} \right\rangle = 4K_a T_n B_r / R_L, \tag{52}$$

or

$$\left\langle i^2_{thermal,1bit} \right\rangle = 4K_a T_n B_r / R_L. \tag{53}$$

Therefore, the thermal noise variance utilizes the absolute noise temperature T_n, electrical bandwidth B_r and load resistance R_L to generate the energy associated with the thermal noise.

The proposed system obtains the modified photocurrent and photocurrent noise variances with the PIIN variance, shot noise variance, and thermal noise variance. The signal-to-noise ratio (SNR) is derived from the energy expressions for the photocurrents (29) and (30) and the photocurrent noise variances (36), (37), (50), (51), (52), and (53). The SNR is given as:

$$SNR_{xbit} = \frac{I^2_{PD,xbit}}{\left\langle i^2_{noise,xbit} \right\rangle}. \tag{54}$$

By comparing $I^2_{PD,xbit}$ and $\langle i^2_{noise,xbit} \rangle$, the SNR of the proposed system can be estimated. This allows the proposed system to measure the BER with equal probability. The BER is determined by the SNR because the Gaussian approximation is used to estimate the BER dependent on the SNR. Therefore, the BER can be expressed as follows [25]:

$$BER = \frac{erfc\left(\sqrt{(SNR_{0bit} \ or \ SNR_{1bit})/2} \right)}{2}. \tag{55}$$

Therefore, the proposed system utilizes the BER to observe various parameters such as the number of simultaneous users, data transmission rate, and effective source power.

TABLE 3. Parameters used in the numerical calculation.

Parameters	Item	Values
PD quantum efficiency	η	0.6
Wavelength location	λ	1.55um
Receiver noise temperature	T_n	300K
Receiver load resistor	R_L	1030Ω

V. NUMERICAL RESULTS

To obtain numerical results, we computed the parameters listed in Table 3, which include the PD quantum efficiency η, wavelength location, data transmission rate, receiver noise temperature T_n, and receiver load resistor R_L. By using 1-D Two-Distinct codes with TCK, we evaluate the performance of the proposed system and compare it to that of other systems utilizing 1-D SP codes with TCK, 1-D BIBD codes, and 1-D BDS codes with TCK.

Figure 4 (a) illustrates the relationship between the BER and the number of simultaneous users using 1-D Two-Distinct codes with TCK, 1-D SP codes with TCK, 1-D BIBD codes, and 1-D BDS codes with TCK with an effective source power P_{sr} of -10 dBm and a data transmission rate of 2.5 Gbps. By setting the BER to 10^{-9}, we can support up to 45 simultaneous users in the proposed system using 1-D Two-Distinct codes with TCK, whereas the other systems using 1-D SP codes with TCK, 1-D BIBD codes, and 1-D BDS codes with TCK can support 26, 12, and 27 simultaneous users, respectively. Therefore, the proposed system using 1-D Two-Distinct codes with TCK outperforms the other systems using 1-D SP codes with TCK, 1-D BIBD codes, and 1-D BDS codes with TCK in terms of supporting simultaneous users. MUI affects the cross-correlation values, which can significantly degrade the system performance. However, the MUI removes the effect of the modified cross-correlation. The modified cross-correlation can improve system performance. Fig. 4 (b) shows the OSNR performance. The OSNR indicates that the number of simultaneous users in the proposed system using 1-D Two-Distinct codes with TCK is large. In contrast, the number of simultaneous users in other systems using 1-D SP codes with TCK, 1-D BIBD codes, and 1-D BDS codes with TCK is small. Nevertheless, the number of simultaneous users in the proposed system using 1-D Two-Distinct codes with TCK exceeds that in other systems using 1-D SP codes with TCK, 1-D BIBD codes, and 1-D BDS codes with TCK.

The graph shown in Fig. 5 illustrates the relationship between the BER and effective source power. It has 45 simultaneous users and a data transmission rate of 2.5 Gbps per user. The effective source power considers the utilization of 1-D Two-Distinct codes with TCK, resulting in a BER of 10^{-9}, for each ONU. Fig. 5 illustrates the effective source power of the 1-D Two-Distinct codes with TCK, which is recorded as -10 dBm. On the other hand, the other systems employing 1-D SP codes with TCK, 1-D BIBD codes, and 1-D BDS codes with TCK achieve effective source powers
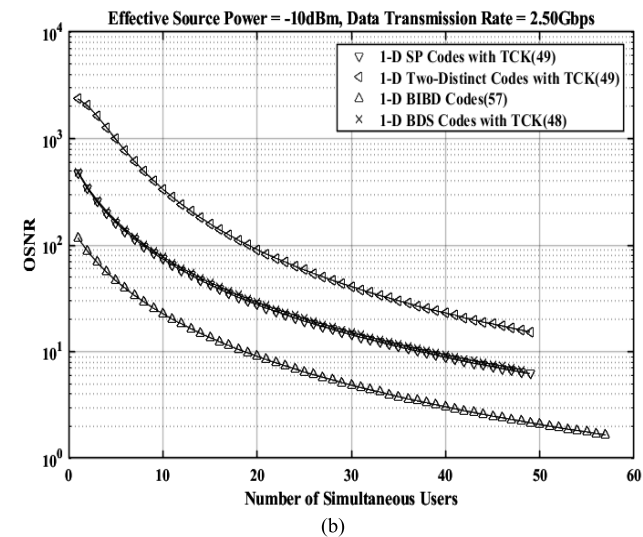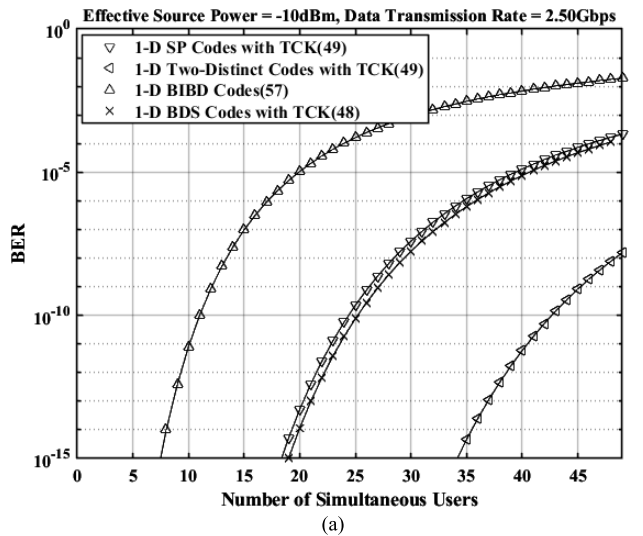
FIGURE 4. (a). Number of simultaneous users versus BER with similar code length of 1-D Two-Distinct codes with TCK. (b). Number of simultaneous users versus OSNR with similar code length of 1-D Two-Distinct codes with TCK.
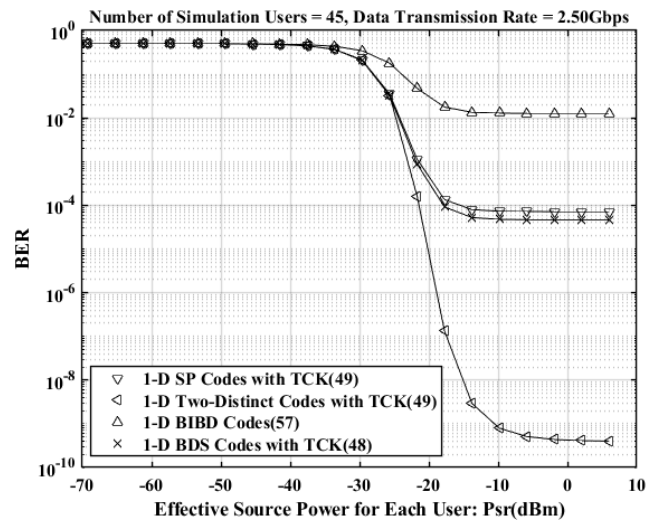

FIGURE 5. Effective source power versus BER with similar code length of 1-D Two-Distinct codes with TCK.
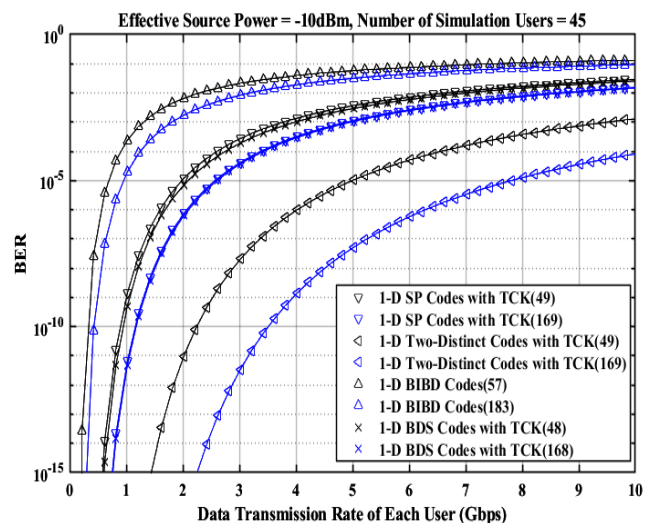
FIGURE 6. Data transmission data versus BER with similar code length of 1-D Two-Distinct codes with TCK.

of -10 dBm at BER of $10^{-4.1}$, $10^{-1.9}$, and $10^{-4.5}$, respectively, as depicted in Fig. 5. The proposed system using 1-D Two-Distinct codes with TCK still outperforms the other systems using 1-D SP codes with TCK, 1-D BIBD codes, and 1-D BDS codes with TCK. In the proposed system using 1-D Two-Distinct codes with TCK, the effective source power needs to exceed -10 dBm to meet the BER requirement of 10^{-9} for each ONU.

Figure 6 shows the BER as a function of the data transmission rate for each user, considering an effective source power of -10 dBm and 45 simultaneous users in black lines. As shown in, the data transmission rate using 1-D Two-Distinct codes with TCK outperforms the other systems using 1-D SP codes with TCK, 1-D BIBD codes, and 1-D BDS codes with TCK. Additionally, the proposed system using 1-D Two-Distinct codes with TCK achieves a data transmission rate of 2.5 Gbps for each user at BER = 10^{-9}, while the

other systems using 1-D SP codes with TCK, 1-D BIBD codes, and 1-D BDS codes with TCK have a BER = 10^{-9} under a data transmission rate of 1Gbps, 0.3Gbps, and 1.05Gbps for each user, respectively. The numerical results show that the proposed system with 1-D Two-Distinct codes with TCK provides better performance in terms of data transmission rate compared to the other systems using 1-D SP codes with TCK, 1-D BIBD codes, and 1-D BDS codes with TCK.

Additionally, in Fig. 6 (blue lines), we present the proposed system that achieves a data transmission rate of 3.9 Gbps with a code weight of 13 using BER = 10^{-9}. Fig. 6 illustrates the proposed system using 1-D Two-Distinct codes with TCK alongside other systems using 1-D SP codes with TCK, 1-D BIBD codes, and 1-D BDS codes with TCK. Fig. 6 reveals that the data transmission rate of the proposed system using

TABLE 4. Overview of the contributions in the performance comparison.

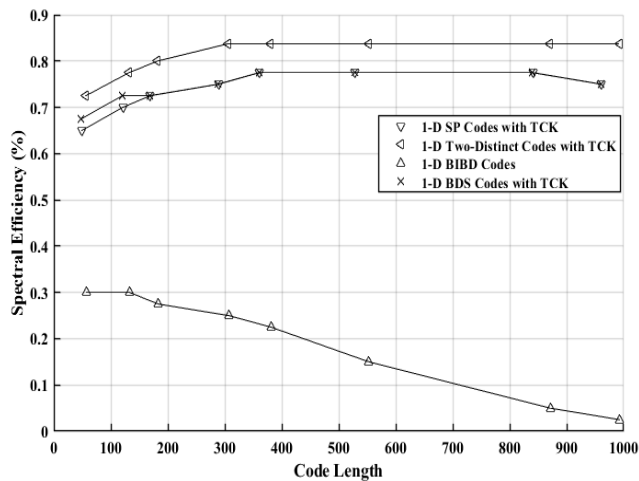|	Number of simultaneous uses	Data transmission rate (similar code length)	Data transmission rate (similar larger code length)	Effective power source	SOP	OCK => TCK
1-D Two-Distinct codes with TCK	Best	Best	Best	Best	Yes	Yes
1-D SP codes with TCK	Good	Good	Good	Good	No	No
1-D BIBD codes	Same	Same	Same	Same	No	No
1-D BDS codes with TCK	Good	Good	Good	Good	No	No

FIGURE 7. Illustrates the relationship between code length and spectral efficiency for SAC-OCDMA systems employing 1-D Two-Distinct codes with TCK, 1-D SP codes with TCK, 1-D BIBD codes, and 1-D BDS codes with TCK.

1-D Two-Distinct codes with TCK exceeds that of other systems utilizing 1-D SP codes with TCK, 1-D BIBD codes, and 1-D BDS codes with TCK.

Figure 7 attains spectral efficiency by utilizing the aggregate information rate and total spectral bandwidth. The spectral efficiency is determined by SE = aggregate information rate/total spectral bandwidth = $\Phi|_{\text{BER}=10^{\wedge}-9}R_b/\Delta f$, where $\Phi|_{\text{BER}=10^{-9}}$ represents the number of simultaneous users at BER = 10^{-9}, and R_b is the data transmission rate per ONU [26]. In Fig. 7, the code length is plotted against the spectral efficiency for SAC-OCDMA systems employing 1-D Two-Distinct codes with TCK, 1-D SP codes with TCK, 1-D BIBD codes, and 1-D BDS codes with TCK. The spectral efficiency achieved with the 1-D Two-Distinct codes using TCK surpasses that of the 1-D SP codes with TCK, 1-D BIBD codes, and 1-D BDS codes with TCK.

Table 4 provides a detailed overview of the contributions of the performance comparison. The number of simultaneous users in the proposed system using 1-D Two-Distinct codes with TCK exceeds that in other systems utilizing 1-D SP codes with TCK, 1-D BIBD codes, and 1-D BDS codes with TCK. With a similar code length, the data transmission rate

in the proposed system using 1-D Two-Distinct codes with TCK is higher than that in other systems employing 1-D SP codes with TCK, 1-D BIBD codes, and 1-D BDS codes with TCK. For a larger code length, we observe that the data transmission rate in the proposed system with 1-D Two-Distinct codes with TCK is higher than that in other systems employing 1-D SP codes with TCK, 1-D BIBD codes, and 1-D BDS codes with TCK. Additionally, the effective power source in the proposed system using 1-D Two-Distinct codes with TCK is lower than that in other systems using 1-D SP codes with TCK, 1-D BIBD codes, and 1-D BDS codes with TCK. In the SOP, we employ two mutually orthogonal SOP to construct the proposed system using 1-D Two-Distinct codes with TCK. However, the other systems utilizing 1-D SP codes with TCK, 1-D BIBD codes, and 1-D BDS codes with TCK do not incorporate the two mutually orthogonal SOP. In the TCK, we utilize the OCK to transition into TCK, thereby achieving the proposed system using 1-D Two-Distinct codes with TCK. In contrast, the other systems employing 1-D SP codes with TCK and 1-D BDS codes with TCK use TCK.

VI. CONCLUSION

This paper proposes a system for SAC OCDMA based on 1-D Two-Distinct codes with TCK. The proposed system employs codes that allow the OLT to use a single BLS to generate two mutually orthogonal SOP, using one with horizontal (0°) polarization and the other with vertical (90°) polarization. The corresponding ONUs are designed for excellent balance properties and simple optical construction, making them easier to implement using available technology. The numerical results demonstrate their ability to improve the BER with the number of simultaneous users in the proposed system using 1-D Two-Distinct codes with TCK. The proposed system with the utilization of 1-D Two-Distinct codes with TCK can support a larger number of simultaneous users (45) compared to the other systems employing 1-D SP codes with TCK, 1-D BIBD codes, and 1-D BDS codes with TCK. The proposed system using the 1-D Two-Distinct codes with TCK in the two mutually orthogonal SOP is capable of maintaining a larger data transmission rate of 2.5 Gbps, in contrast to the other systems employing 1-D SP codes with TCK,

1-D BIBD codes, and 1-D BDS codes with TCK. The proposed system employing the 1-D Two-Distinct codes with TCK can operate with a lower effective source power of -10 dBm compared to the other systems utilizing 1-D SP codes with TCK, 1-D BIBD codes, and 1-D BDS codes with TCK. Therefore, we propose the use of 1-D Two-Distinct codes with TCK in SAC-OCDMA systems to divide two mutually orthogonal SOP of the proposed ONUs(τ) into two code keying of the proposed photodiodes.

ACKNOWLEDGMENT

REFERENCES

[1] S. Abd El-Mottaleb, H. Fayed, A. Abd El-Aziz, M. Metawee, and M. Aly, "Enhanced spectral amplitude coding OCDMA system utilizing a single photodiode detection," *Appl. Sci.*, vol. 8, no. 10, p. 1861, Oct. 2018.

[2] A. Jurado-Navas and A. Puerta-Notario, "Generation of correlated scintillations on atmospheric optical communications," *J. Opt. Commun. Netw.*, vol. 1, no. 5, pp. 452–462, 2009.

[3] A. Stok and E. H. Sargent, "Comparison of diverse optical CDMA codes using a normalized throughput metric," *IEEE Commun. Lett.*, vol. 7, no. 5, pp. 242–244, May 2003.

[4] H. M. R. Al-Khafaji, S. A. Aljunid, and H. A. Fadhil, "Improved BER based on intensity noise alleviation using developed detection technique for incoherent SAC-OCDMA systems," *J. Modern Opt.*, vol. 59, no. 10, pp. 878–886, Jun. 2012.

[5] M. Moghaddasi, S. Seyedzadeh, I. Glesk, G. Lakshminarayana, and S. B. A. Anas, "DW-ZCC code based on SAC–OCDMA deploying multi-wavelength laser source for wireless optical networks," *Opt. Quantum Electron.*, vol. 49, no. 12, pp. 393–406, Dec. 2017.

[6] M.-S. Alouini, A. Abdi, and M. Kaveh, "Sum of gamma variates and performance of wireless communication systems over nakagami-fading channels," *IEEE Trans. Veh. Technol.*, vol. 50, no. 6, pp. 1471–1480, Nov. 2001.

[7] D. Kakati and S. C. Arya, "Performance of 120 Gbps single channel coherent DP-16-QAM in terrestrial FSO link under different weather conditions," *Optik*, vol. 178, pp. 1230–1239, Feb. 2019.

[8] A. Jurado-Navas, C. Álvarez-Roa, M. Álvarez-Roa, and M. Castillo-Vázquez, "Cooperative terrestrial-underwater wireless optical links by using an amplify-and-forward strategy," *Sensors*, vol. 22, no. 7, p. 2464, Mar. 2022, doi: 10.3390/s22072464.

[9] C. Álvarez-Roa, M. Álvarez-Roa, F. J. Martín-Vega, M. Castillo-Vázquez, T. Raddo, and A. Jurado-Navas, "Performance analysis of a vertical FSO link with energy harvesting strategy," *Sensors*, vol. 22, no. 15, p. 5684, Jul. 2022.

[10] F. Xu, M.-A. Khalighi, and S. Bourennane, "Impact of different noise sources on the performance of PIN- and APD-based FSO receivers," in *Proc. 11th Int. Conf. Telecommun.*, Jun. 2011, pp. 211–218.

[11] A. Bekkali, T. D. Pham, K. Kazaura, K. Wakamori, and M. Matsumoto, "Performance analysis of SCM-FSO links for transmission of CDMA signals under gamma–gamma turbulent channel," in *Proc. IEEE Mil. Commun. Conf.*, Oct. 2009, pp. 1–5.

[12] S. A. A. El-Mottaleb, A. Métwalli, M. Hassib, A. A. Alfikky, H. A. Fayed, and M. H. Aly, "SAC-OCDMA-FSO communication system under different weather conditions: Performance enhancement," *Opt. Quantum Electron.*, vol. 53, no. 11, pp. 616–633, Nov. 2021.

[13] V. A. Aalo, "Performance of maximal-ratio diversity systems in a correlated nakagami-fading environment," *IEEE Trans. Commun.*, vol. 43, no. 8, pp. 2360–2369, Aug. 1995.

[14] J. W. Goodman, *Statistical Optics*. New York, NY, USA: Wiley, 1985.

[15] A. Jurado-Navas, J. M. G. Balsells, J. F. Paris, and A. Puerta-Notario, "A unifying statistical model for atmospheric optical scintillation," in *Numerical Simulations of Physical and Engineering Processes*, J. Awrejcewicz, Ed. Rijeka, Croatia: IntechOpen, 2011, ch. 8, pp. 181–206, doi: 10.5772/25097.

[16] J. Wang, J.-Y. Yang, I. M. Fazal, N. Ahmed, Y. Yan, H. Huang, Y. Ren, Y. Yue, S. Dolinar, M. Tur, and A. E. Willner, "Terabit free-space data transmission employing orbital angular momentum multiplexing," *Nature Photon.*, vol. 6, no. 7, pp. 488–496, Jun. 2012.

[17] Z. Wei, H. M. H. Shalaby, and H. Ghafouri-Shiraz, "Modified quadratic congruence codes for fiber Bragg-grating-based spectral-amplitude-coding optical CDMA systems," *J. Lightw. Technol.*, vol. 19, no. 9, pp. 1274–1281, Sep. 2001.

[18] J. Garrido-Balsells, A. Jurado-Navas, J. Paris, M. Castillo-Vázquez, and A. Puerta-Notario, "On the capacity of M-distributed atmospheric optical channels," *Opt. Lett.*, vol. 38, no. 2, pp. 3984–3987, 2013.

[19] D. Neves, A. Sanches, R. Nobrega, H. Mrabet, I. Dayoub, K. Ohno, S. Haxha, I. Glesk, A. Jurado-Navas, and T. Raddo, "Beyond 5G fronthaul based on FSO using spread spectrum codes and graphene modulators," *Sensors*, vol. 23, no. 8, p. 3791, Apr. 2023. [Online]. Available: https://www.mdpi.com/1424-8220/23/8/3791

[20] H. M. R. Al-Khafaji, S. A. Aljunid, A. Amphawan, H. A. Fadhil, and A. M. Safar, "Reducing BER of spectral-amplitude coding optical code-division multiple-access systems by single photodiode detection technique," *J. Eur. Opt. Soc., Rapid Publications*, vol. 8, p. 13022, Mar. 2013.

[21] W. Sahraoui, A. Amphawan, S. Berrah, and R. Matem, "A novel 2D polarization-spatial encoding approach for OCDMA system based on multi-core fiber," *Optik*, vol. 228, Feb. 2021, Art. no. 166164.

[22] H. S. Zaeer Dhaam, F. M. Ali, and A. G. Wadday, "Evaluation performance of two-dimensional multi-diagonal code using polarization and wavelength of OCDMA system," *Al-Furat J. Innov. Electron. Comput. Eng.*, vol. 1, no. 3, p. 22, Sep. 2020.

[23] C.-C. Yang, "Optical CDMA passive optical network using prime code with interference elimination," *IEEE Photon. Technol. Lett.*, vol. 19, no. 7, pp. 516–518, Apr. 1, 2007.

[24] Z. Wei and H. Ghafouri-Shiraz, "Codes for spectral-amplitude-coding optical CDMA systems," *J. Lightw. Technol.*, vol. 20, no. 8, pp. 1284–1291, Aug. 2002.

[25] C. C. Yang, "Spectral amplitude coding optical CDMA networks using $2^m \times 2^m$ waveguide gratings," *IEEE Photon. Technol. Lett.*, vol. 22, no. 24, pp. 1835–1837, Dec. 15, 2010.

[26] T.-W. Frederick Chang and E. H. Sargent, "Optimizing spectral efficiency in multiwavelength optical CDMA system," *IEEE Trans. Commun.*, vol. 51, no. 9, pp. 1442–1445, Sep. 2003.

BIH-CHYUN YEH received the B.S., M.S., and Ph.D. degrees in communication engineering from National Taiwan University, Taipei, Taiwan, in 1996, 1998, and 2009, respectively. From 2009 to 2010, he was a Postdoctoral Fellow with the Research Center for Information Technology Innovation, Academia Sinica, under the guidance of Dr. De-Nian Yang. From 2011 to 2019, he joined as a Faculty Member of Chang Gung University, where he was an Assistant Professor.

In 2019, he joined as a Faculty Member of Chang Gung University, where he is currently an Associate Professor. His research interests include OCDMA encoding/decoding codes and security, wire and wireless communication systems, error control coding, digital cameras, video and audio processing hardware, biomedical engineering communication, neural and fuzzy networks, and IC design.

• • •